Static Response Calibration of 3D Printed Thin Walled Structures Using Fused Deposition Modelling

By

Akhilesh Kulkarni

Presented to the Faculty of Graduate School of

The University of Texas at Arlington in Partial Fulfillment

Of the Requirements

For the Degree of

MASTER OF SCIENCE IN MECHANICAL ENGINEERING

THE UNIVERSITY OF TEXAS AT ARLINGTON

December 2019

Acknowledgements

I would like to thank Dr. Robert Taylor for mentoring and guiding me throughout my coursework and being a constant source of motivation. I would also like to thank Dr. Ashfaq Adnan and Dr. Amir Ameri for providing me with their valuable feedback and for allowing me to use their lab equipment as and when necessary.

I would like to thank Mr. Rhugdhrivya Rane for helping me in the tensile tests and 3-point bending tests. I am thankful to Mr. Edgar Mares for helping in cantilever tests and setting hyper mesh models. I would like to acknowledge the Mechanical and Aerospace Engineering Department of University of Texas at Arlington for providing a great opportunity. I would like to extend my gratitude to my family for being supportive of my academic pursuits.

November 25, 2019

Abstract

Static Response Calibration of 3D Printed Thin Walled Structures Using Fused Deposition Modelling

Akhilesh Kulkarni, MS

The University of Texas at Arlington, 2019

Supervising Professor: Dr. Robert Taylor

3D printing has enabled flexible, tool-less fabrication that yields numerous benefits. One benefit is unique and complex structural arrangements that increase design freedom to minimize weight. Such arrangements can be guided by advanced topology, shape, and sizing optimization tools using appropriate process constraints to ensure a printable design and can include highly integrated structural details such as stiffeners, flanges, frames, and other connections.

3D printing thin wall aircraft structures presents challenges for material and structural characterization. 3D printing enables integrated structural details, each detail is affected by the print process capability to fabricate the local geometry and deviations from designed geometry and structural connectivity can result in quite different structural capability from the design intent.

The present work seeks to characterize the effect of print orientation on static response of thin wall structures using calibration factors on local geometric details. The approach is implemented using a wide stiffened beam printed using Fused Deposition

Modeling (FDM). This work adds an equivalent stiffness analytical model to predict beam performance. An analytical model has been developed for a stiffened beam representation that has been calibrated with coupon test data that incorporates print orientation effects. The calibrated analytical model results are compared with the actual experimental test results, FE results. In addition, the calibrated analytical model is compared with the results obtained using published mechanical properties from the Stratasys for ABS M30. The calibrated analytical model shows better results than the published values in comparison to experimental and FE results.

Table of Contents

Contents

List of Figures

List of Tables

Chapter 1 Introduction

3D printing technologies has enabled us to design and fabricate complex systems and components those were unattainable previously which in return has opened many new opportunities to study the technology. The 3D printed technologies have given the power to manufacture/prototype any part/model with less cost and time to manufacture. This technology is reducing the product development time from weeks to days because of its simplicity and ability to produce complex products. The 3D printing technology has made its way to manufacture the wind tunnel models for aerodynamic and aeroelastic evaluation of aircraft configurations.

One such opportunity lies on small aircrafts where 3D printing has provided fast and toll less fabrication. One of the benefits of 3D printing is it gives freedom to design and develop complex systems which can help reduce the weight with the same structural applications as other manufacturing processes provides. The design to minimize weight can be guided by advanced topology, shape and sizing optimization tools using appropriate process constraints to ensure the designs can include structural details such as stiffeners, flanges, frames and other connections.

With the opportunities comes challenges and those must be overcome in order to achieve successful implementation and maximize the use of 3D orienting technology. Currently, most aircrafts use thin wall nature structures which are best suited for the lightweight aircraft. Whereas most 3D orienting technologies have enough thickness to enable raster or fill pattern. The stiffened panel used in aircrafts are often thin wall structures which a slicing algorithm cannot replicate for 3D printing and yields in

unpredictable material continuity e.g. internal voids and gap in external contours. Depending on the 3D printing technology used print process parameters such as print orientation, bead overlap, print speed, layer thickness and other process parameters can have significant effect on accuracy and structural integrity of printed thin wall structures.

3D printing thin wall aircrafts structures presents challenges for material and structural characterization. Much work has been done to characterize mechanical properties of 3D printed materials, many process effects are not manifested in mechanical property studies and only show up at the structural scale [1] [2] [3] [4] [5] [6] [7] [8] [9]. Apart from studies to demonstrate similarity to laminated plate theory much less work has been done to characterize for structural response accounting for 3D printing process parameters [10] [11] [12]. For thin walled structures, material and structural response to 3D printing process parameters and its effects becomes a subject of concern because less materials is available at a particular location to overcome local defects and process effects. Additionally, each geometric detail is affected by the print process, and deviations from designed geometry and connectivity can result in quite different structural response from design point of view. These effects become much more important since these ate transfers in load transfer across the joints and can be seen in structural behavior when partial infill is used in structural member.

Structural characterization must examine the effects on structural response in process specific approach. In Addition, structural studies must examine the geometric specific effects induced by the specific 3D printing process. This is the approach in this work to examine the structural response for a 3D printing process.

The present work seeks to characterize the effect of print orientation on static response of thin wall structures using calibration factors on local geometric details. The approach is implemented using stiffened beam printed using Fused Deposition Modelling (FDM). The work builds on previous work which compared the finite element response to experimental response but neglected the coupon level process effects. This work adds an equivalent stiffness analytical model to predict beam performance. It further adds coupon level mechanical data to calibrate analytical and finite element model structural response for the print orientation.

Chapter 2 Background

The present work to calibrate static response of thin wall structures builds upon concepts and methods for fabrication, modeling, and weight minimization of thin wall structures. These topics are discussed below.

2.1 Additive Manufacturing

Manufacturing techniques are constantly evolving to resolve the current manufacturing issues and serve better in terms of form, fit and function. Manufacturers around the world are looking for manufacturing techniques which are cost effective and easy to implement. Additive Manufacturing (AM) is one such technique which allows for design freedom and can fabricate complex shapes. In AM, a CAD model is used to fabricate the desired product in layer by layer fashion like laminates using either plastic material or metal powder. AM is a digital manufacturing technique which is different than a traditional mold manufacturing, which is costly, complex and time consuming. [13]

As the name suggest AM-Additive Manufacturing, material is added and not subtracted like conventional manufacturing processes where the material is removed to get the final product and/or is then assembled to get the desired product. This technology enables us to save on material and reduces the manufacturing time. In addition, it allows designing of the complex geometries such as internal features, undercuts etc. [13]

There are different ways to classify AM technologies. A popular approach is according to technology used i.e. power source used, printer technology, extrusion technology. Currently adopted classification from ASTM F42 and ISO 261 as per follows,

1. Vat Photopolymerization: Liquid polymer is processed by delivering energy to cure specific regions
2. Powder Bed Fusion: Container filled with powder which is exposed to energy source typically laser or electron beam
3. Material Extrusion: Deposits material layer by layer by extruding through a heated nozzle
4. Material Jetting: ink-jet printing process
5. Binder Jetting: binder is printed into a powder bed in order to form cross sections
6. Sheet Lamination: Material in sheet form deposited layer by layer
7. Directed Energy Deposition: Processes that simultaneously deposit material and energy through a single deposition device. [14]

The general additive manufacturing process follows eight steps in which a computer aided drawing (CAD) is converted into actual physical product. The key steps in the process are:

1. Conceptualization and CAD model
2. Conversion to STL/AMF
3. Transfer and manipulation of STL/AMF file on AM machine
4. Machine Setup
5. Build
6. Part removal and cleanup
7. Post processing of part
8. Application

Fused Deposition Modelling technique was used in this work to study the effect of print orientation to characterize the mechanical response of the part. [14]

2.2 Fused Deposition Modeling

Fused Deposition Modelling (FDM) or Fused Filament Modelling (FFF) is by far the most common extrusion-based system, produced and developed by Stratasys. [14]

2.2.1 Operation:

FDM uses heating chamber to semi-liquify polymer that is fed into the extruder with specific size of nozzle diameter as a filament. The filament is pushed into the extruder by a wheel arrangement which generates the extrusion pressure. The extrusion head moves in x-y direction while depositing the material on the build surface. The axis movement is programmed as either the bed moves downwards, or the head moves upwards to deposit material. Nozzle diameters can vary from 0.01 to 0.05 in. [13]

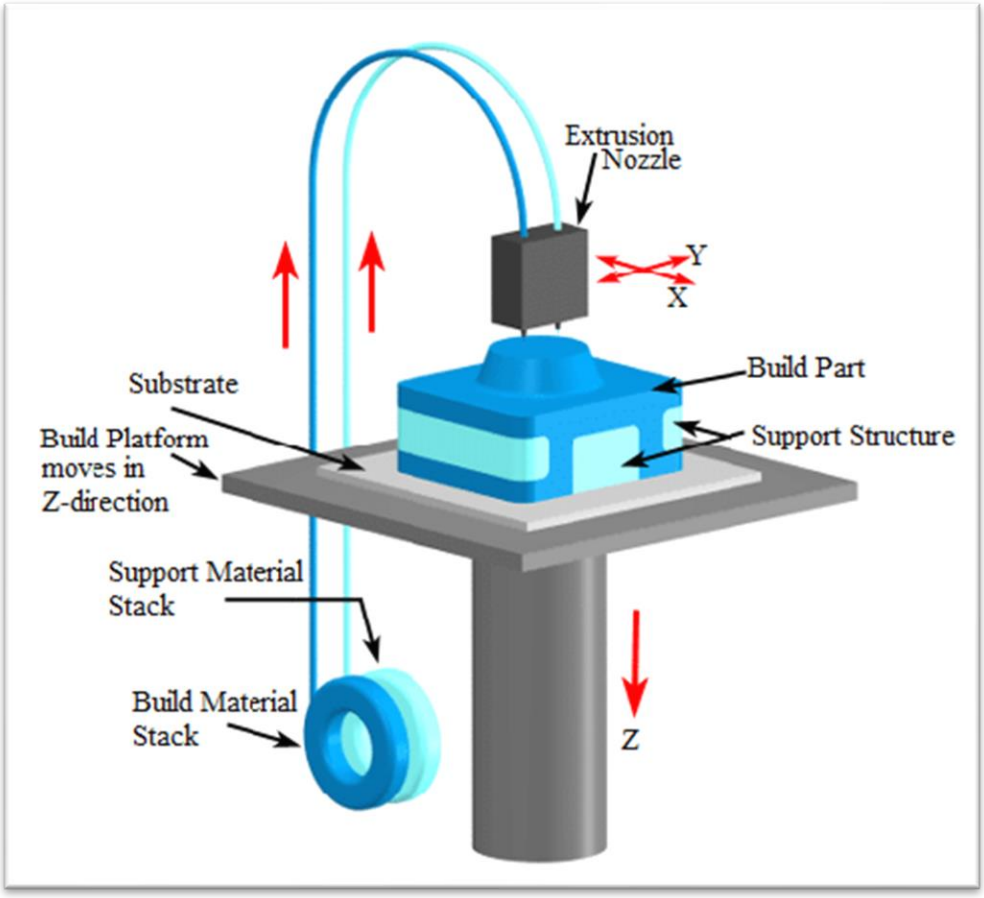

Figure 1-Schematic of FDM process [15]

Every manufacturing process has its advantages and disadvantages. The main advantage is this process can use wide range of materials that are available. The most popular material is ABS (Acrylonitrile Butadiene Styrene). The disadvantages of using the FDM technique is in terms of build speed, accuracy and material density. In addition, the important design consideration to use FDM technology is the final products anisotropic nature. [14]. Different layering strategies can have different strengths. Typically, the part properties are isotropic in x-y direction and they tend to change in z-direction i.e. build

direction. The z-direction is relatively low compared to x-y plane direction. Not only is build speed a major drawback but also the size of the machines, more specifically the build volume. The largest being the Objet10003, which has a build tray of 1000 x 800 x 500 mm, created by Stratasys. [16]

2.3 Design and Optimization of Thin Walled Structure

3D printing technologies provide both the advantages and disadvantages to fabricate aircraft and aerodynamic structures. First, these technologies provide design freedom to develop complex stiffeners configurations to have directional stiffening effect.

This complexity can be through cross sectional configuration (wall thickness or continuously variable cross-sectional shape) or structural arrangement (directional or iso-grid) or skin thickness distribution. Some of the examples of thin walled structures are shown in Figure 2. Further design freedom can be applied through different engineering materials such as fiber reinforcement of deposited polymer beads.

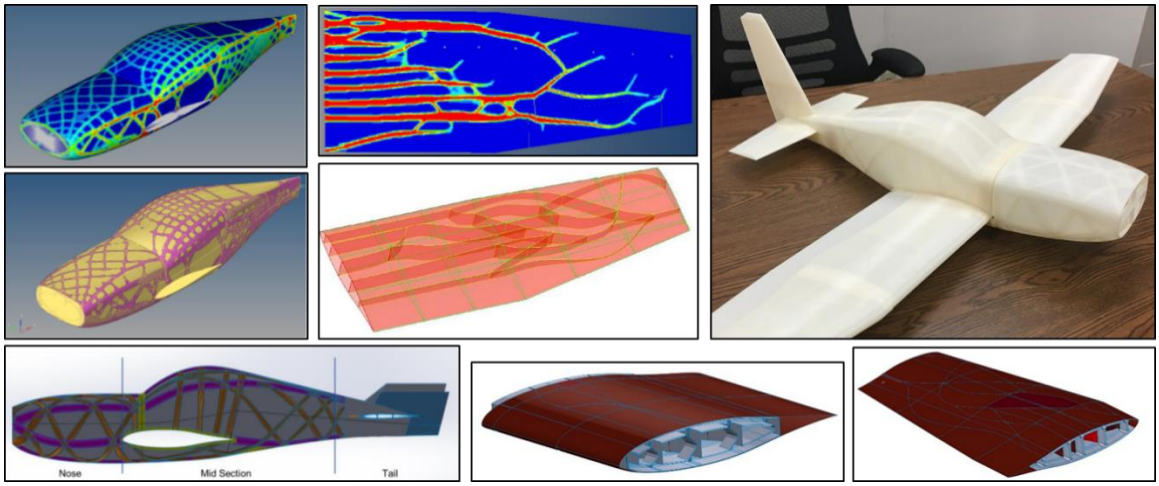

Figure 2-Examples of stiffness tailoring by geometric complexity enabled by 3D printing [17]

These technologies offer some constraints on fabrication that must be considered while designing the aircraft model. FDM technology converts the polymeric feedstock into a 3D geometry using a layer by layer deposition in which each layer is fabricated in particular direction. This process of sequential and directional fabrication of material can affect the material capability i.e. anisotropy, voids, weak bonds between layers) and geometric capability (e.g. overhangs and bridges). This accounting includes design restrictions that incorporate strength and stiffness as a function of 3D printing process parameter such as build orientation and wall thickness.

As process knowledge is incorporated into automated optimization tools, designers can design a lightweight structured aircraft to push innovative design. Process limitation can provide opportunities for technology development as discussed below for z-direction strength improvement in FDM process.

2.4 Fabrication of Thin Wall FDM Structures

Each 3D printing technology shared some common material characterization. One such common characteristic is the reduced strength of fabricated part in build i.e. z-direction. The layering process in 3D printed components creates voids and geometrical discontinuity causes to differ mechanical and physical properties compared to bulk material. Some polymer 3D printing processes shows z-direction strength can be an order of magnitude lower than in-plane strengths. [18]

In FDM process the reduced strength occurs transvers to deposited polymer tracks, which have interface strength that vary based on the thermal gradient during the build process. Voids at the directional changes produces stress areas which can initiate bond failure at static or very low fatigue levels.

This material inhomogeneity in FDM parts not only creates strength variations but also stiffness variation. As shown in Figure 3, deposited beads have rounded corners that creates void at bead corners. The size of voids depends on 3D printing process parameters and determines amount of contact between successive layers. Because of these effects the material continuity is not 100% and the developed modulus in not equal to bulk material modulus.

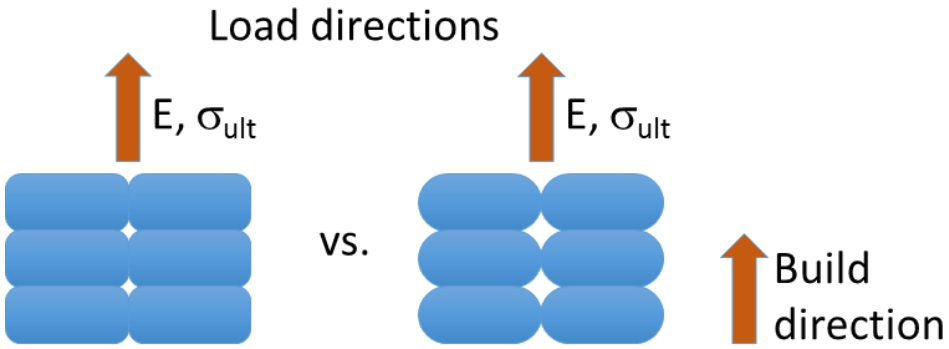

Figure 3-Effect of bead interface on material continuity

Additionally, a key trade off in printing process can achieve desirable mechanical properties. This trade of can affect the geometric accuracy of the fabricated part. One such adjustment is, in FDM process, increased overlap between deposited material can cause higher inter-bead bond strength and reduces chances because of directional changes voids. However, the overlap increases the amount of material deposited, it must spread outside the boundaries of desired contours. In thin wall 3D printed FDM structure, stiffener effectiveness depends on inter-bead bond strength and geometric accuracy. Figure 4 shows the cross section with out of the boundaries with build direction.

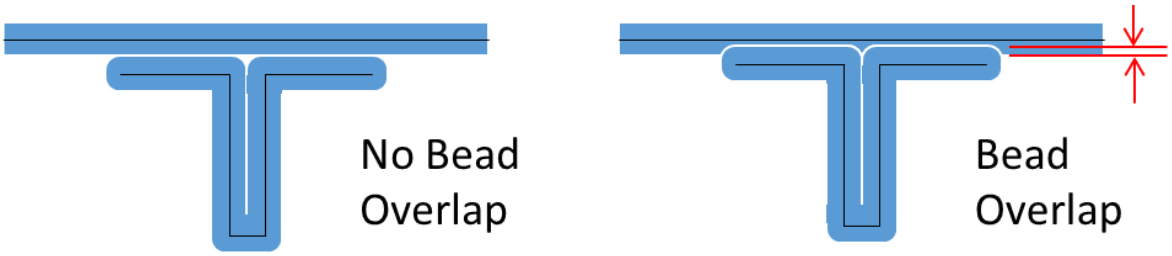

Figure 4-Effect of bead overlap on local stiffener continuity

The structural performance of the thin wall structure shown in Figure 2 depends on the effectiveness of thin structures such as shown in Figure 3-Effect of bead interface on material continuity, which have angles relative to 3D printing build direction that vary considerably. The effect of print orientation on local stiffener can be shown in Figure 5 A stiffener printed vertically aligns each bead on top of bead exactly below with no gap. The spacing between bead is immediately adjacent to next. The material continuity in 45^0 build orientation further reduces by creating a fap between the adjacent beads. At this print angles, only half of the bead is in contact with the bead below and spacing between the beads is 1.414 times apart because of identical surface spacing. This spacing leaves the gap in-between the beads. This gap results in further modulus reduction in these features.

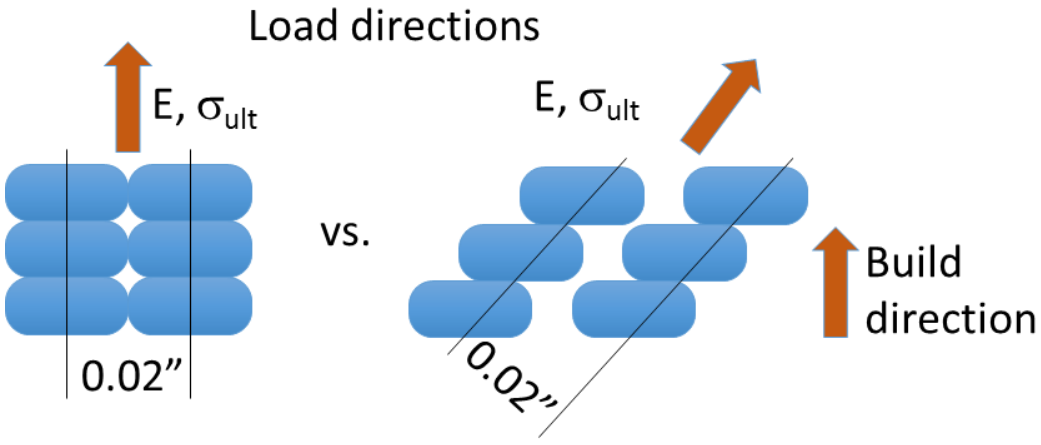

Figure 5-Effect build orientation on local stiffener material continuity

The present work involves initial testing and modeling to develop and validate a methodology for accounting the build orientation effect shown in Figure 5 on local stiffener material continuity and part stiffness. Such stiffness calibration is needed in order to

facilitate elastic scaling suitable for 3D printed aeroelastic wind tunnel models to match aeroelastic test behavior using engineered 3D printed materials to tune and tailor model performance.

Chapter 3 Methodology

An approach to characterize the effect of print orientation on static response of thin wall structure using calibration of local geometric details is implemented using a wide stiffened beam printed using FDM. The following sections discuss the beam study model and previous fabrication, modelling and test results from this model [19]. In further sections, coupon level mechanical test data is presented which is used to calibrate the analytical model and finite element model structural response for print orientation effect. Finally, an equivalent stiffness analytical model is presented that is calibrated with local detail stiffness factors to predict the beam static response.

3.1 Stiffened Beam Model

To investigate the effects of 3D print orientation on stiffness and flexural behavior of a thin wall structure, a stiffened beam model was defined. [19] The plate is 10 inches long by 3.33 inches wide, and 0.5 inches deep with two stiffening arrangements, 0^0 and 45^0 stiffeners, as shown in Figure 6-00 and 450 stiffening configurations in beam model Figure 6-00 and 450 stiffening configurations in beam model

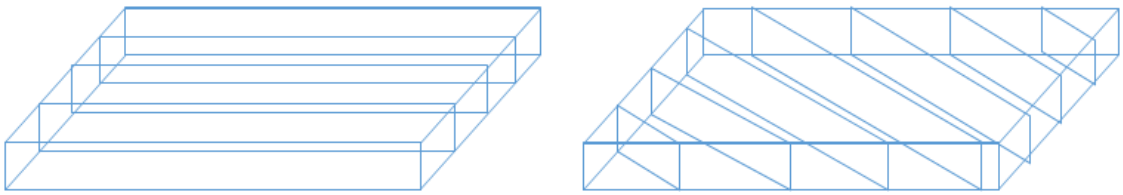

Figure 6-0^0 and 45^0 stiffening configurations in beam model

Printed bead thickness is 0.02 inches for settings used on the Stratasys Fortus 450MC using ABS-M30 material. Beads are printed 0.02 inches apart to and defined using surface models as shown Figure7-2 and 4 bead 00 stiffened beam model cross section Figure7 for the 0º stiffened plate. Skin thickness of the scaled plate is 2 print beads. Stiffener thickness effect is studied at two different thicknesses, 2 beads and 4 beads.

Figure7-2 and 4 bead 0^0 stiffened beam model cross section

3.2 3D Print Orientation Effect

To establish the effect of build orientation on the scaled stiffened plate flexural modulus, the plate is fabricated in two orientations, vertical and 45º, as shown in Figure 8 and Figure 9. As discussed previously, bead overlap and spacing at the inclined print angle affects material continuity and thus the developed stiffness in the fabricated geometry. These effects are illustrated in the sliced stiffener geometry as the part is prepared for printing. The vertical build develops adjacent beads while the 45º build develops a gap between beads.

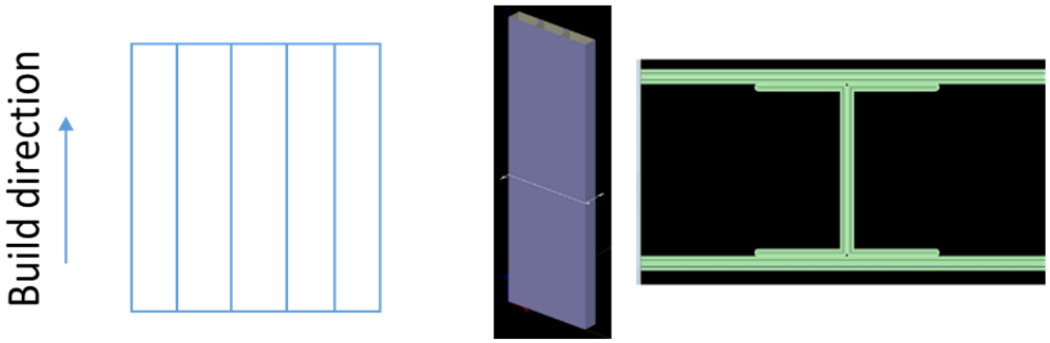

Figure 8-Build orientation (vertical)

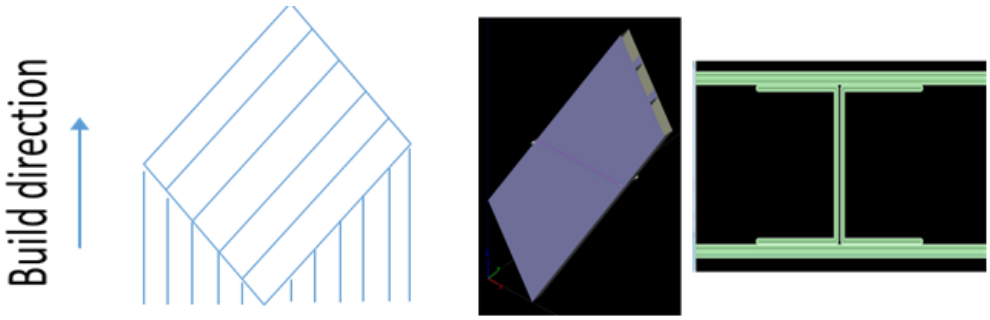

Figure 9-Build orientations 45^0 for beam model

The scaled plate models were 3D printed on a Stratasys Fortus 450MC, in both the 90º and 45º build orientations as shown in Figure 10. Several stabilizing walls were required to support the 45º oriented plates during the print. A total of 8 plates were printed: 0º stiffened with 2 beads per stiffener, 0º stiffened with 4 beads per stiffener, 45º stiffened with 2 beads per stiffener, 45º stiffened with 4 beads per stiffener. Stiffener material continuity is best in 90º prints for the 0º stiffened plates and best in 45º prints for the 45º stiffened plates.

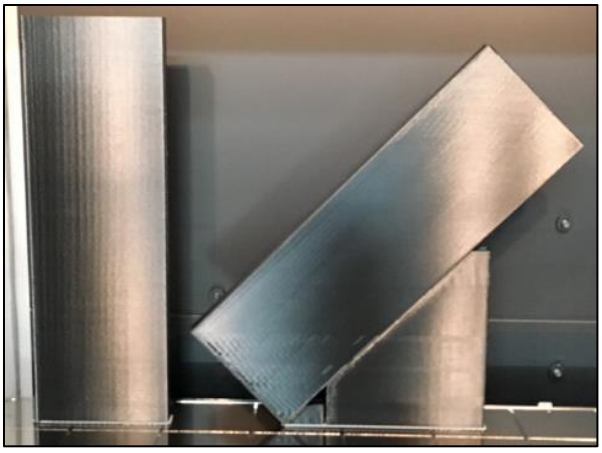

Figure 10-Stratasys Fortus 450MC actual printed beam models

3.3 Coupon Testing

3.3.1 Test Specimen Design

The specimens were designed on Solidworks using a modified version of ASTM D638-02a standards as shown in Figure 11. The final design was saved as a .STL file format which was later used as the input for the slicing software.

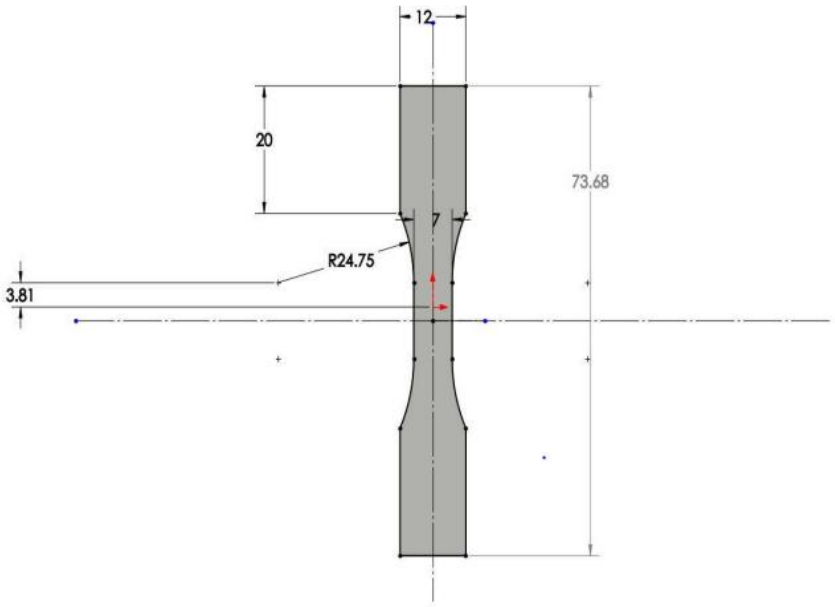

Figure 11-Coupon specimen design [13]

3.3.2 Coupon Testing

To establish the effect of build orientation on the scaled plate flexural modulus, the plate is fabricated in two orientations, vertical and 45^0, as shown in figure. The print angle affects the material continuity and thus affects the stiffness in the fabricated model. To take this variation in stiffness into consideration for the mathematical formulation, 3 ASTM D638 test specimens were printed each at 90^0 (vertical) and 45^0 (Inclined) orientations on a Stratasys Fortus 450MC as shown in Figure 12 below. Stabilizing walls were required to support the 45^o oriented plates during the print. Printed bead thickness is 0.02 inches for settings used on the Stratasys Fortus 450MC using ABS-M30 material. Beads are printed 0.02 inches apart and defined using surface models of the specimens with no contour beads. Testing for the two coupon configurations was carried out on a Shimadzu Autograph model AGS-X universal testing machine.

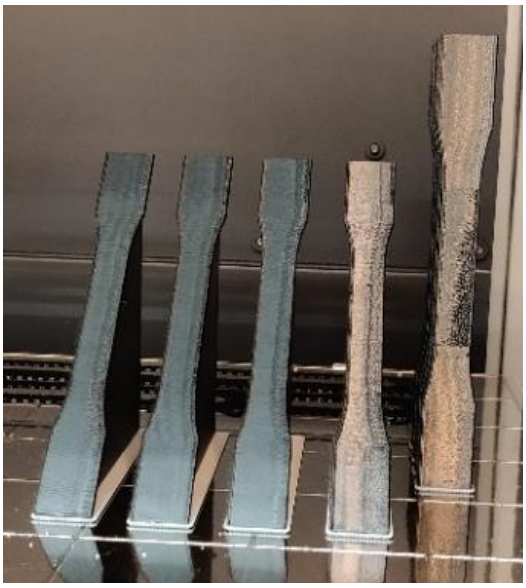

Figure 12-3D printed 90^0 and 45^0 test specimens and test configurations

4 bead specimens were tested with bead thickness 0.02 inches apart. Figure 13 shows the bead separation of the tensile specimens.

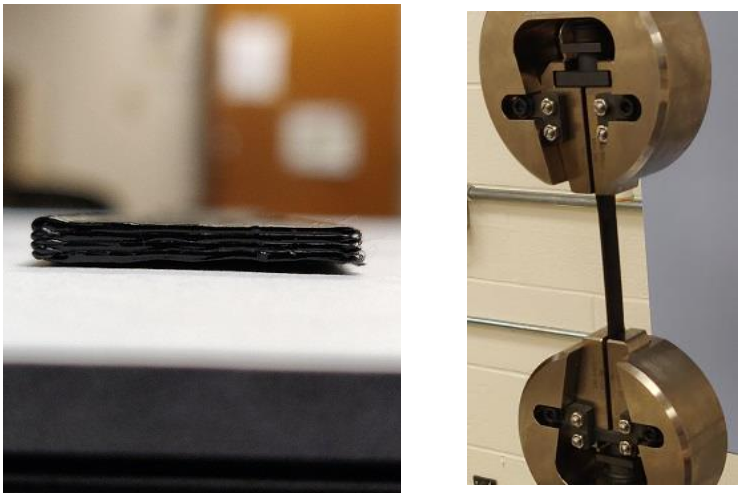

Figure 13-(a) Tensile test coupons with 4 bead arrangement and (b)ensile test of coupons on Schimadzu AGS-X universal testing machine

The test is performed as per ASTM D638 and modulus of elasticity was calculated for the two coupon configurations. Stress vs. strain plots for 4 coupon configurations are shown below and indicate significant modulus and strength reduction for the angled print.

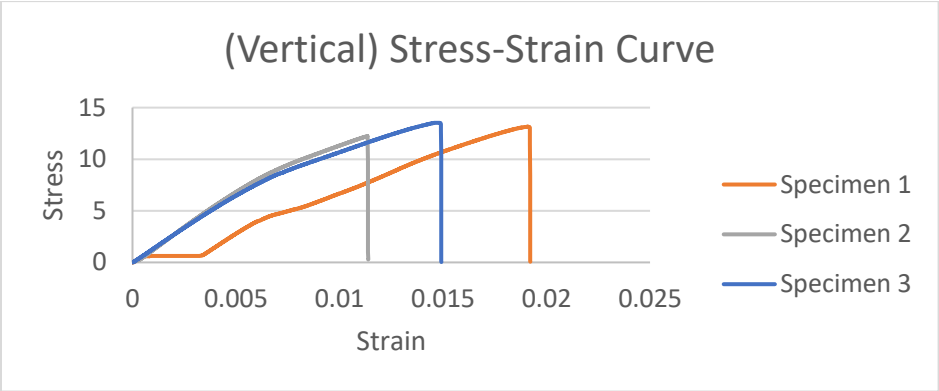

Figure 14-Stress vs Strain plots

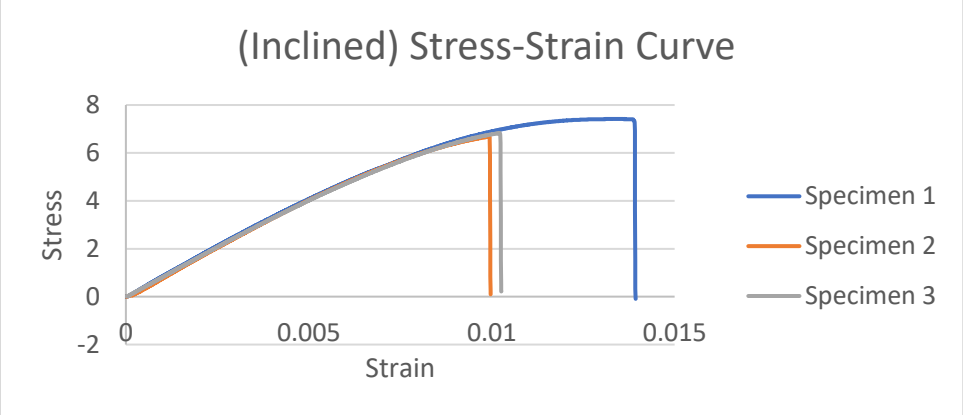

Figure 15-Stiffener Stress vs Strain plots

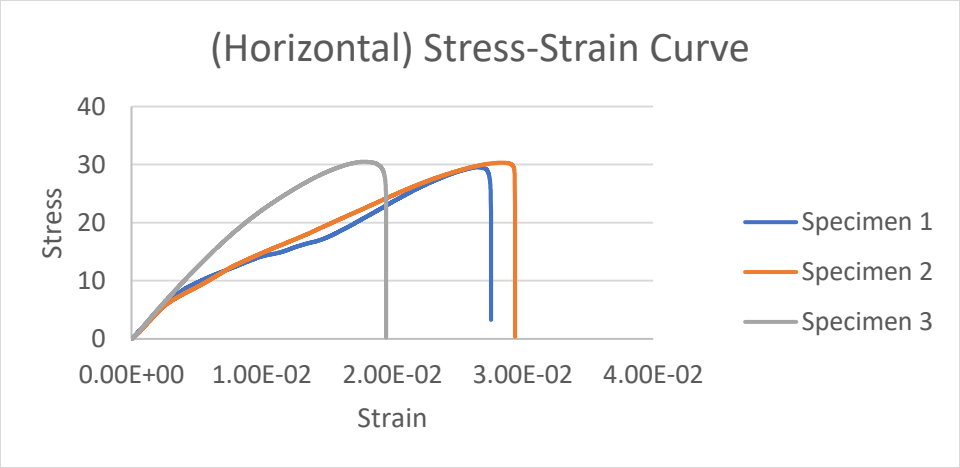

Figure 16-Horizontal Stress vs Strain plots

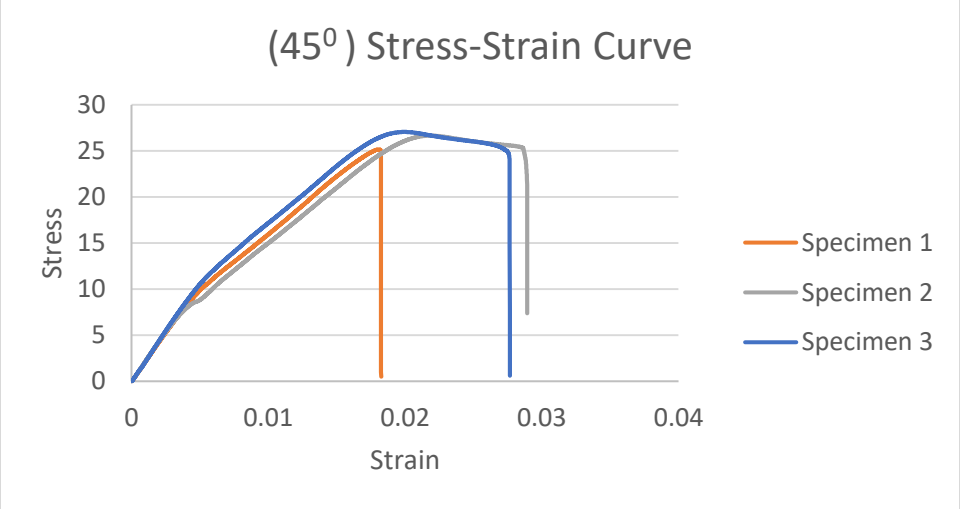

Figure 17-45^0 orientation print Stress vs Strain plots

3 coupons were tested for each case above and then average values were calculated to use in mathematical formulation discussed in the sections that follow.

Table 1-Modulus values from coupon test data

Vertical print modulus				Horizontal Print Modulus			
Specimen 1 (MPa)	Specimen 2 (Mpa)	Specimen 3 (Mpa)	Avg (Mpa)	Specimen 1 (MPa)	Specimen 2 (Mpa)	Specimen 3 (Mpa)	Avg (Mpa)
747.83	856.18	1035.31	879.773	1223.37	979.62	1769.7	1324.2
45^0 skin moduli				Inclined (Stiffener modulus)			
Specimen 1 (MPa)	Specimen 2 (Mpa)	Specimen 3 (Mpa)	Avg (Mpa)	Specimen 1 (MPa)	Specimen 2 (Mpa)	Specimen 3 (Mpa)	Avg (Mpa)
1147.439	1253.21	1227.14	1209.26	543.37	707.87	686.72	646

3.3 Mathematical Formulation

An equivalent plate stiffness approach [20] is used to obtain the relation between stress and strain of the entire plate. [ABD] matrices are be formulated for entire plate summing contributions from each geometric entity. The laminate stiffness matrix equations are derived from classical laminated plate theory. The stress strain relation is given by,

$$\begin{bmatrix} N \\ M \end{bmatrix} = \begin{bmatrix} A & B \\ B & D \end{bmatrix} \begin{bmatrix} \varepsilon_0 \\ \chi \end{bmatrix} \quad 1$$

Where,

[N]= Force matrix

[M]= Moment matrix

[A]= Extensional stiffness matrix

[B]= Extensional-Bending stiffness

[D]= Bending stiffness matrix

[ε_0] = Mid-plane strains

[χ]= Mid-plane curvatures of the plate

The [ABD] matrices are given by,

$$[A] = \int [Q] dh \qquad [B] = \int [Q] h dh \qquad [D] = \int [Q] h^2 dh \qquad 2$$

3.3.1 [D] Matrix calculations:

The D matrix determines bending response in the analytical model of the plate. The D matrix terms depend on the cube of the distance between each section of the plate and the mid-plane of the plate. The mathematical expression for the bending matrix is given by,

$$[D] = \int [Q]\, h^2 dh$$

Where $[Q]$ is reduced stiffness matrix. Hence, the D matrix for the plate is given by,

$$[D]_{plate} = [D]_{skin} + [D]_{stiffener} + [D]_{flange} \qquad 3$$

The D matrix is thus calculated for each section of the plate: skin, stiffeners, and flanges. Modulus values are adjusted as appropriate based on values determined from the coupon testing.

$$[D]_{skin} = \begin{bmatrix} D_{11} & D_{12} & 0 \\ D_{21} & D_{22} & 0 \\ 0 & 0 & D_{66} \end{bmatrix} \quad 4$$

Where,

$$D_{11} = 2.\left[\frac{(E_1)^2}{E_1 - E_2.(\nu_{12})^2}\right].(h)^3_{skin}$$

$$D_{12} = D_{21} = 2.\left[\frac{-\nu_{12}.E_1.E_2}{E_1 - E_2.(\nu_{12})^2}\right].(h)^3_{skin}$$

$$D_{22} = 2.\left[\frac{E_1.E_2}{E_1 - E_2.(\nu_{12})^2}\right].(h)^3_{skin}$$

$$D_{66} = 2.[G_{12}].(h)^3_{skin}$$

$$[D]_{stiffener} = \begin{bmatrix} D_{11} & D_{12} & D_{16} \\ D_{21} & D_{22} & D_{26} \\ D_{61} & D_{62} & D_{66} \end{bmatrix} \quad 5$$

Where,

$$D_{11} = \frac{E.I}{d_\theta}.m^4$$

$$D_{12} = D_{21} = \frac{E.I}{d_\theta}.m^2.n^3$$

$$D_{16} = D_{61} = \frac{E.I}{d_\theta}.m^3.n6$$

$$D_{22} = \frac{E.I}{d_\theta}.n^4$$

$$D_{26} = D_{62} = \frac{E.I}{d_\theta}.m.n^3$$

$$D_{66} = \frac{E.I}{d_\theta}.m^2.n^2$$

$$[D]_{flange} = \begin{bmatrix} D_{11} & D_{12} & D_{16} \\ D_{21} & D_{22} & D_{26} \\ D_{61} & D_{62} & D_{66} \end{bmatrix} \quad 6$$

Where,

$$D_{11} = \frac{E.I_{flange}}{d_\theta}.m^4$$

$$D_{12} = D_{21} = \frac{E.I_{flange}}{d_\theta}.m^2.n^3$$

$$D_{16} = D_{61} = \frac{E.I_{flange}}{d_\theta}.m^3.n$$

$$D_{22} = \frac{E.I_{flange}}{d_\theta}.n^4$$

$$D_{26} = D_{62} = \frac{E.I_{flange}}{d_\theta}.m.n^3$$

$$D_{66} = \frac{E.I_{flange}}{d_\theta}.m^2.n^2$$

Where,

$I =$ Moment of inertia of stiffeners

$$I = \frac{w.h_{stiffeners}^3}{12}$$

$I_{flange} =$ Moment of inertia of flange section

m= cos θ; n= sin θ

The [Q] matrix from equation (2) for skin arrangement and stiffener arrangement is obtained by stress and strain relation matrix, which is given below

[ε]=[S][**σ**]

Where, [ε] = strain matrix

[**σ**] = stress matrix and,

[S] = compliance matrix = $[Q]^{-1}$

$$[S] = \begin{bmatrix} 1/E_x & -\nu_{yx}/E_y & \eta_{sx}/G_{xy} \\ -\nu_{xy}/Ex & 1/E_y & \eta_{sy}/G_{xy} \\ \eta_{xs}/E_x & \eta_{ys}/E_y & 1/G_{xy} \end{bmatrix} \quad 7$$

The engineering constants in the matrix are,

E_x= Modulus in x-direction

E_y= Modulus in y-direction

G_{xy}= Shear Modulus in x-y plane

η_{xs} and η_{sy}, are the ratios of the normal strains ε_x and ε_y to the shear strain Υ_s respectively

ν_{xy} = stress in the x-direction and strain in the y-direction similarly for ν_{yx}

All the terms of the [S] matrix can be calculated using following equation:

$$\frac{1}{E_x} = \frac{m^2}{E_1}(m^2 - n^2\nu_{12}) + \frac{n^2}{E_2}(n^2 - m^2\nu_{21}) + \frac{m^2n^2}{G_{12}} \quad (8)$$

$$\frac{1}{E_y} = \frac{n^2}{E_1}(n^2 - m^2\nu_{12}) + \frac{m^2}{E_2}(m^2 - n^2\nu_{21}) + \frac{m^2n^2}{G_{12}} \quad (9)$$

$$\frac{1}{G_{12}} = \frac{4m^2n^2}{E_1}(1 + \nu_{12}) + \frac{4m^2n^2}{E_2}(1 + \nu_{21}) + \frac{m^2-n^2}{G_{12}} \quad (10)$$

$$\frac{\nu_{xy}}{E_x} = \frac{\nu_{yx}}{E_y} = \frac{m^2}{E_1}(m^2\nu_{12} - n^2) + \frac{n^2}{E_2}(n^2\nu_{21} - m^2) + \frac{m^2n^2}{G_{12}} \quad (11)$$

$$\frac{\eta_{xs}}{E_x} = \frac{\eta_{sx}}{G_{xy}} = \frac{2m^3n}{E_1}(1 + \nu_{12}) - \frac{2mn^3}{E_2}(1 + \nu_{21}) - \frac{mn(m^2-n^2)}{G_{12}} \quad (12)$$

$$\frac{\eta_{ys}}{E_y} = \frac{\eta_{sy}}{G_{xy}} = \frac{2mn^3}{E_1}(1 + \nu_{12}) - \frac{2m^3n}{E_2}(1 + \nu_{21}) + \frac{mn(m^2-n^2)}{G_{12}} \quad (13)$$

Where,

E_1= Modulus in Horizontal direction

E_2= Modulus in vertical direction

G_{12}= Shear Modulus in 1-2 plane

ν_{12} = stress in the horizontal-direction and strain in the vertical-direction similarly for ν_{21}

m= cos θ and n=cos θ

where, θ= print orientation angle

G_{12} was calculated using $\frac{1}{E_x}$ equation where E_x is modulus in 45^0 print orientation, and E_1 and E_2values are taken from the tensile coupon test data to calculate the unknown term G_{12}. This value of G_{12} is then used to calculate rest of the terms of the matrix for all the arrangements. [21]

3.3.2 Deflection calculations for the scaled plate model

3 point bending and cantilever beam configurations are modeled for the stiffened beam as discussed below. A laminated beam solution following [22] is used to solve for 3-point bend deflection. For the stiffened beam model, the classical formulas must be modified to account for the 3-D printed build orientations and to consider the angle of the stiffeners and number of stiffeners. The theory assumes that the length is much larger than the width i.e. L >> b. The bending stiffness EI is replaced by equivalent stiffness $E_x^b I$ defined by,

$$E_x^b I = \sum_{k=1}^{N} E_l^k I^k \qquad 14$$

For bending of symmetric plates, the relationship between moments and curvature at mid-plane is given by,

$$\begin{bmatrix} M_x \\ M_y \\ M_{xy} \end{bmatrix} = \begin{bmatrix} D_{11} & D_{12} & D_{16} \\ D_{12} & D_{22} & D_{26} \\ D_{16} & D_{26} & D_{66} \end{bmatrix} \begin{bmatrix} \chi_x \\ \chi_y \\ \chi_{xy} \end{bmatrix} \qquad 15$$

Inverting the above equation,

$$\begin{bmatrix} \chi_x \\ \chi_y \\ \chi_{xy} \end{bmatrix} = \begin{bmatrix} D_{11}^* & D_{12}^* & D_{16}^* \\ D_{12}^* & D_{22}^* & D_{26}^* \\ D_{16}^* & D_{26}^* & D_{66}^* \end{bmatrix} \begin{bmatrix} M_x \\ M_y \\ M_{xy} \end{bmatrix} \quad 16$$

Where

D_{ij}^* are elements of the inverse matrix of D_{ij}.

D_{ij} is bending or flexural laminate stiffness relating moments to curvature.

The curvatures are defined as,

$$\chi_x = -\frac{\partial^2 w}{\partial x^2} \quad ; \qquad \chi_y = -\frac{\partial^2 w}{\partial y^2} \quad ; \qquad \chi_{xy} = -2.\frac{\partial^2 w}{\partial x.\partial y}$$

In order to apply the beam theory, following assumptions are made:

$$M_x = M_{xy} = 0 \quad 17$$

From (1), (2) and (8), we get

$$\chi_x = -\frac{\partial^2 w}{\partial x^2} = D_{11}^*.M_x \quad 18$$

Assuming beam have a high length to width ratio, it is assumed that,

$$w = w(x) \quad 19$$

Caution must be taken in applying above equation since for unsymmetrical plates the curvatures χ_x and χ_{xy} are the functions of bending moment M_x which is given by,

$$\chi_y = -\frac{\partial^2 w}{\partial x^2} = D_{12}^*.M_x; \qquad \chi_{xy} = -2.\frac{\partial^2 w}{\partial x.\partial y} = D_{16}^*.M_x \quad 20$$

Thus, the deflection w cannot be independent of y. In case of shear coupling, the term D_{16} in equation 20 induces the twisting curvature can cause the specimen to lift off its supports at the corners. [22] This phenomenon is negligible when R (length-to-width ratio) is large, which is the assumption made at the start of developing this model.

After integrating equation (18) twice and applying boundary conditions we get

$$w = D_{11}^{*}.\frac{P.L^3}{48} \quad 21$$

For cantilever test the equation becomes,

$$w = D_{11}^{*}.\frac{P.L^3}{3} \quad 22$$

3.4 Finite Element Analysis of the beam

The scaled 3D printed stiffened plate models were modeled in Hyper Mesh. When using Hyper Mesh there are re some assumptions which need to be considered while modelling. The software assumes that there is perfect bonding between the layers and adjacent bead, but in actual scenario that is not the case.

The modulus calculate from the coupon testing are used to run the models in software to account for the 3D print orientation effect. The Hyper Mesh models were created using shell models to represent the thin surfaces and beads of the 3D printed models.

The cross section of the model is shown in Figure 18 below

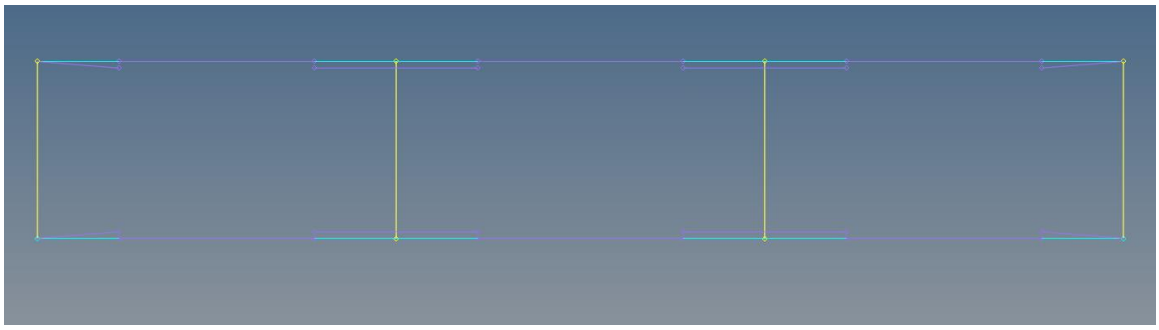

Figure 18 - Cross section of the plate model in Hyper mesh

As the model is created it is then meshed to quad and triangular mesh. 0^0 scaled model is meshed with quad elements and 45^0 is meshed with combination quad and triangular mesh.

The model can be separated into categories for each surface. The purple colored surfaces represent the exterior surface thickness. The blue colored surface represents the flanges on the stiffeners. Lastly, the yellow colored surfaces represent the stiffeners. These colored surfaces are illustrated in the 0^0 scaled stiffened plate model shown in Figure 19 and the 45^0 scaled stiffened plate model. [16]

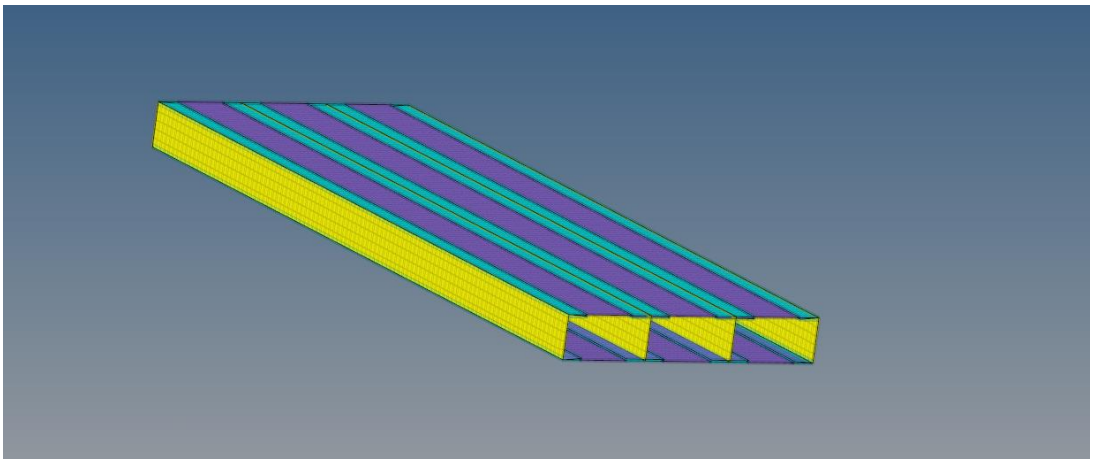

Figure 19 - 3D model of the plate in Hyper mesh

As shown in Figure 19, these categories of surfaces are given a thickness corresponding to the original scaled 3D printed plate. The thicknesses correspond to 26 the dimensions stated in section 3.1. Flange and surface regions of the model used z-offsets to correctly position the thickness. [16]

The material is ABS M30 which is created in the software, but as stated earlier to replicate the actual plate behavior the material properties used are from the coupon tests. E.g. the model will be assigned the vertical, 45^0 stiffener material properties and 45^0 material property for the skin, respectively.

The table shows the material properties for the respective print orientation.

Table 2 - ABS M30 Mechanical Properties in ZX axis [23]

Mechanical Properties	**Value**	**Units**
Tensile Strength, Yield	3,750	psi
Tensile Strength, Strength	4050	psi
Tensile Modulus	310000	psi
Poissons Ratio	0.35	
Elongation at Break	2%	
Elongation at yield	1%	

In the cantilever bend test the top and bottom surface on one end is completely fixed. The constraints were defined by fixing all degrees of freedom (DOF 123456). To apply a single point force at the end of the plate and along the edge, a single node which was made using RBE3 was generated. Displacement results were extracted from the tip midpoint on the top surface. [16]

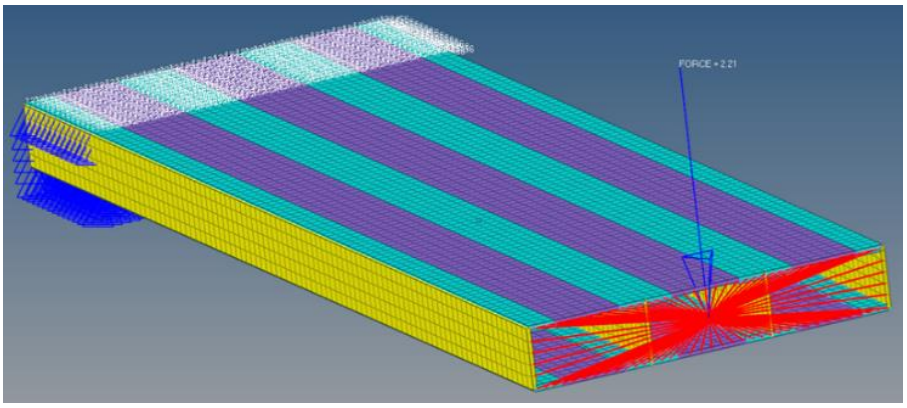

Figure 20 - 3D model of the plate in Hypermesh with applied load and constraints for cantilever beam

On the other hand, the 3-point bend test has two constraints on the bottom surface near the ends of the plate. The constraints spaced at seven inches apart were defined by fixing translation (DOF 123). The upper surface has four loads acting at each stiffener to simulate the total force applied in a 3-point bend test.

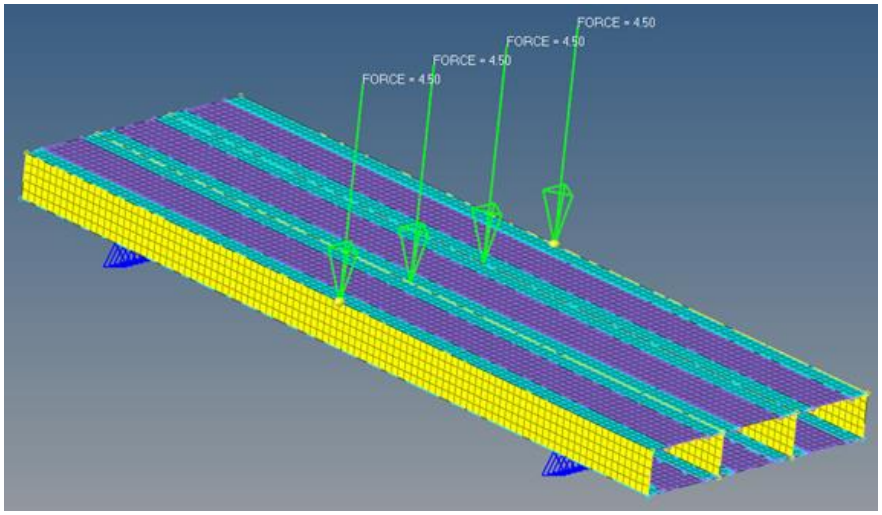

Figure 21 - 3D model of the plate in Hypermesh with load and constraints applied for 3-point bend test

3.5 Plate Testing

To investigate the mechanical behavior of the plates, two different tests were performed. The 3-point bend test and cantilever tests were performed for the 3D printed plates. Both tests rely on modulus, making them ideal to determine the mechanical behavior in the plates.

Two beam bending configurations are studied in order to test and calibrate for process-induced stiffness effects. For a 3-point bend configuration as shown in Figure 22, Euler-Bernoulli beam theory predicts transverse displacement to be $w = \frac{PL^3}{48EI}$. For a cantilever beam configuration, as shown in Figure 23, beam theory predicts transverse displacement to be $w = \frac{PL^3}{3EI}$.

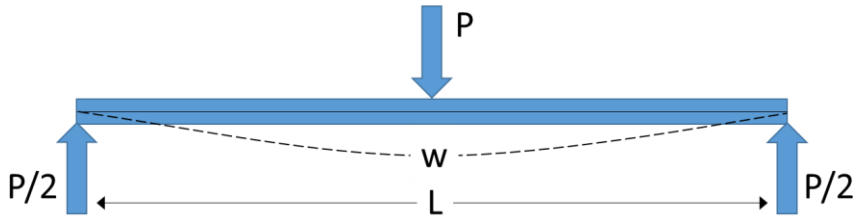

Figure 22-3-point bend free body diagram and deflection

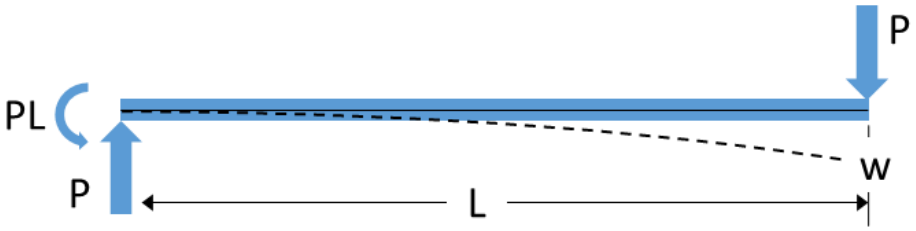

Figure 23-Cantilever beam free body diagram and deflection

3.5.1 Cantilever Beam Test

The scaled 3D printed plates were clamped to the table while the other end had weight of one kilogram applied shown in Figure 24. Previous work [19] executed 3 point bend experimental tests, and finite element simulation, for the 3D printed 0º- and 45º stiffened beams. The analytical formulation for the cantilever test is derived in the previous section 3.3.2 Deflection calculations for the scaled plate model for the similar set of models. The mathematical formulation results will be then compared to the experimental results later section to validate the mathematical formulation.

Figure 24- (a) Cantilever bending test (b) -3 Point bending test

3.5.2 3-Point Bending Test

Previous work [19] executed 3 point bend experimental tests, and finite element analysis for 3 point bending test which are updated with coupon test data, for the 3D printed 0^{o}-stiffened beams. Those results are compared with the analytical results in next section.

Chapter 4 Results

In previous work [19] the experimental tests conducted in order the understand the effect of bead thickness, geometric configuration and 3D print orientation on stiffness of the plate.

This work adds the analytical model to compare the effect of coupon level testing and compares it with the experimental testing and computational results. In addition, the analytical results are calculated for the published values for ABS M30 from Stratasys. [23] The analytical results of published values are then compared with the equivalent stiffness model to evaluate the effect of 3D print orientation.

The current work presents a methodology for accounting for print orientation effects on stiffness in modeling structural response of FDM-printed thin wall structures. An analytical model has been developed for a stiffened beam representation that has been calibrated with coupon test data that incorporates print orientation effects. Additionally, existing finite element models have been updated with coupon test data to complete validation of the analytical models.

First, the results of FE models are compared with test results and FE results with modified modulus from the test coupons. The Table 3 and Figure 25 compares the test results, FE results from modified modulus and FE results from published values. [23]

Table 3 - Result Table - FE results and test results comparison

FE comparison with Test					
Configuration	**Test Displacement (inches)**	**FE displacement-Modified (inches)**	**FE displacement-Published Material Properties (inches)**	**% difference (Test vs FE Modified)**	**% difference (Test vs FE Published)**
3 Point Bend Test					
2 bead, 90° print	0.027	0.046	0.01933	-70.37	28.41
2 bead, 45° print	0.034	0.034	0.02679	0.00	21.21
4 bead, 90° print	0.025	0.039	0.01618	-56.00	35.28
4 bead, 45° print	0.028	0.034	0.02243	-21.43	19.89
Cantilever Test					
2 bead, 90° print	0.090	0.134	0.05541	-48.89	38.43
2 bead, 45° print	0.101	0.104	0.07669	-2.97	24.07
4 bead, 90° print	0.083	0.1217	0.05013	-46.63	39.60
4 bead, 45° print	0.090	0.083	0.06947	7.78	22.81
Cantilever Test (45^0 stiffeners)					
2 bead, 90° print	0.161	0.1788	0.07238	-11.06	55.04
2 bead, 45° print	0.155	0.1661	0.1003	-7.16	35.29
4 bead, 90° print	0.136	0.1279	0.0679	5.96	50.07
4 bead, 45° print	0.127	0.119	0.094	6.30	25.98

Column 5 and column 6 from Table 3 compares the % difference between the Test Vs FE Modified and Test Vs FE Published results. It is seen that the FE Published results underestimates deflection as compared to test displacement and most of the FE modified results overestimates the displacement. This is mainly because the published values stiffness is more than the actual plate structure stiffness and the stiffness obtained

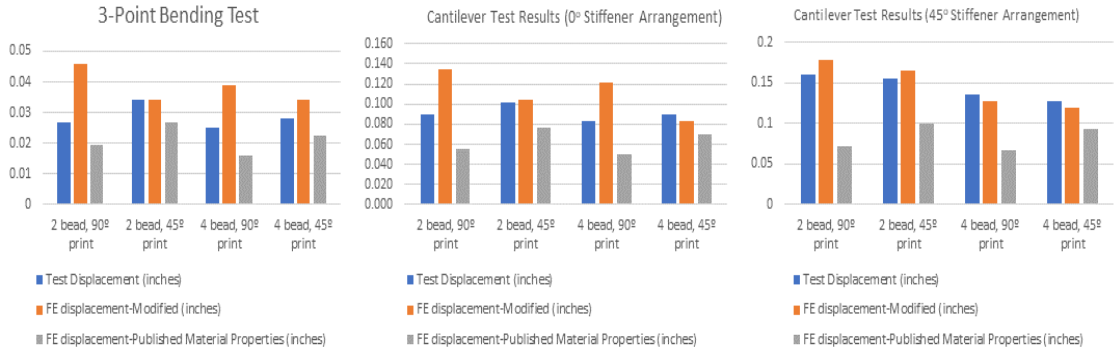

Figure 25-Bar chart showing comparison for Test and FE Displacement

from tensile test coupons is less than the actual stiffness of plate structure. The reasons can be as follows:

1. Different printing process parameters than the process parameters used for printing of actual plates.
2. Errors in testing of the tensile coupons and actual 3-point bend test and cantilever test
3. Machine Error for all the tests (including calibration error) since the displacements are very small
4. It is very difficult to replicate the plate level structure, e.g. bead overlap and bead joint at coupon level, so the stiffness of coupons is less than the overall plate structure.
5. Bead to bead gap in tensile coupons was not uniform as it is shown in Figure 26 below

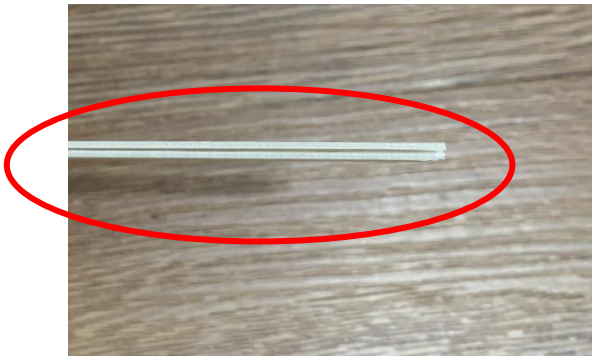

Figure 26-Gap between beads for tensile coupons

6. Assumptions in analytical model:
    a. The model assumes that the length is very large as compared to width, but it is not the case
    b. G_{12} is not calculated experimentally rather it is calculated using various equations

For two 2-bead, 90^o print and 4-bead, 90^o (0^0 Stiffener arrangement) the % variation is more for the FE modified than the FE published. For other configurations, the FE modified values are closer to the test results as compared to FE published results.

Similarly, Analytical results are compared with the test results in Table 4. The column 4 and column 5 in the Table 4 gives the % difference between Analytical-Modified vs Test and Analytical-Published Vs Test. From the table it is seen that apart from the two-configuration stated above i.e. 2-bead, 90^o print and 4-bead, 90^o (0^0 Stiffener arrangement) the Analytical-Modified results are much closer than Analytical-Published results. This shows that the analytical model accounts for the effect of print orientation on the stiffness of the plate structure.

The bar chart comparing all the results shown in Table 4 is shown below.

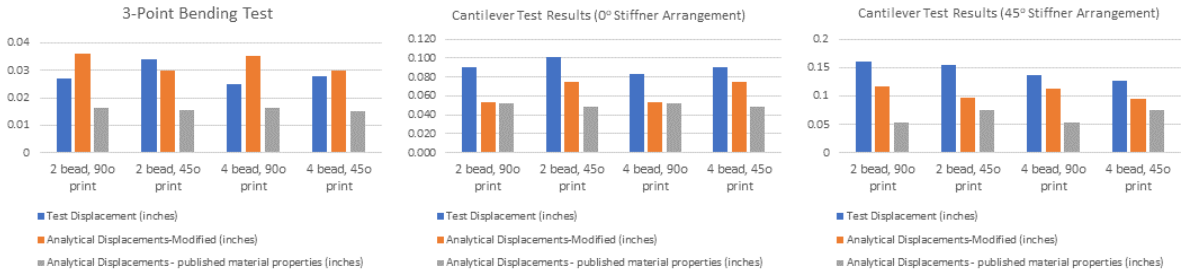

Figure 27- Bar chart comparing results for Test and Analytical Displacement

From Figure 27 , it can be seen that the analytical published values are very different than the Test and Analytical-Modified displacement which shows that the analytical model considers the effect of 3-D print orientation.

Table 4 - Result Table – Analytical results and test results comparison

Configuration	Test Displacement (inches)	Analytical Displacements- Modified (inches)	Analytical Displacements - published material properties (inches)	% difference Analytical (Test vs Analytical - Modified)	% difference Analytical (Test vs Analytical - Published)
3 Point Bend Test					
2 bead, 90º print	0.027	0.036	0.0164	-33.33	39.26
2 bead, 45º print	0.034	0.030	0.0154	11.88	54.71
4 bead, 90º print	0.025	0.035	0.0162	-41.48	35.20
4 bead, 45º print	0.028	0.030	0.0150	-6.57	46.43
Cantilever Test					
2 bead, 90º print	0.090	0.05373	0.0527	40.30	41.44
2 bead, 45º print	0.101	0.07494	0.049	25.80	51.49
4 bead, 90º print	0.083	0.054	0.0521	35.54	37.23
4 bead, 45º print	0.090	0.07518	0.0481	16.47	46.56
Cantilever Test (45º stiffeners)					
2 bead, 90º print	0.161	0.116	0.0535	27.95	66.77
2 bead, 45º print	0.155	0.096	0.0749	38.10	51.68
4 bead, 90º print	0.136	0.1132	0.0537	16.76	60.51
4 bead, 45º print	0.127	0.0955	0.07518	24.80	40.80

Table 5 – Comparison of FE, Analytical and Test Results

Configuration	FE displacement-Modified (inches)	Analytical Displacements-Modified (inches)	Test Displacement (inches)
3 Point Bend Test			
2 bead, 90º print	0.046	0.036	0.027
2 bead, 45º print	0.034	0.030	0.034
4 bead, 90º print	0.039	0.035	0.025
4 bead, 45º print	0.034	0.030	0.028
Cantilever Test			
2 bead, 90º print	0.134	0.05373	0.090
2 bead, 45º print	0.104	0.07494	0.101
4 bead, 90º print	0.1217	0.054	0.083
4 bead, 45º print	0.083	0.07518	0.090
Cantilever Test (45º stiffeners)			
2 bead, 90º print	0.1788	0.116	0.161
2 bead, 45º print	0.1661	0.096	0.155
4 bead, 90º print	0.1279	0.1132	0.136
4 bead, 45º print	0.119	0.0955	0.127

Table 5 compares the results of FE-Modified, Analytical-Modified, and actual Test displacements. The results are easy to visualize and compare in the format of bar charts. The bar chart for each test configurations are plotted and shown below. From Figure 28 it can be seen that all the results for 3-Point bend test are very much close to each other with some error in test displacement results specially for 2 beads, 90º print configuration.

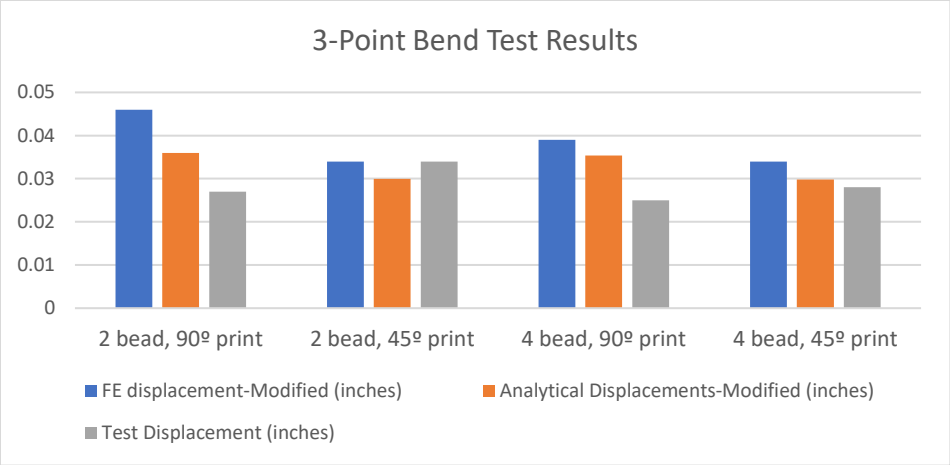

Figure 28-Bar chart - 3 Point bend test result comparison

The next plot is for cantilever test with 0^o stiffener arrangement. The results for 2-bead, 90^o print configuration for 0^o stiffener arrangement seems to offset i.e. the difference is large for Analytical-Modified, FE-Modified and Test results. For other configuration it seems that the FE-Modified, Analytical-Modified and Test results do not show that much larger difference. More detail work is needed to see why there is so much difference particularly for 0^o stiffener arrangement with 90^o print configuration.

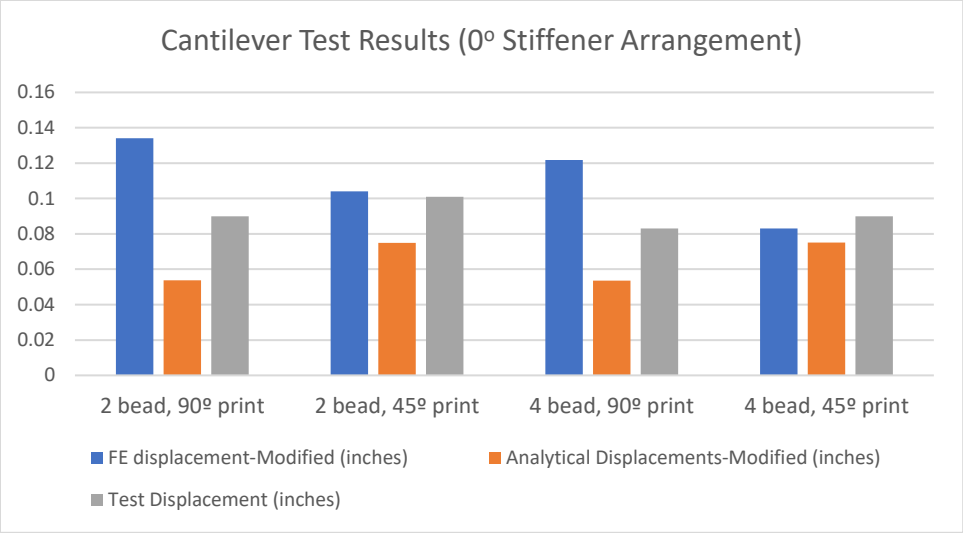

Figure 29-Cantilever Test results comparison (0º Stiffener arrangement)

The last plot compares all the results for cantilever tests with 45º stiffener arrangement. The comparison form Figure 30 shows that there is some error in the 2 bead 90º and 45º print configurations. For the 4 bead print configurations the analytical displacements-modified are very much closer with the test and FE modified results. More work is required to identify why the 2 bead analytical results are farther than the FE modified and test results.

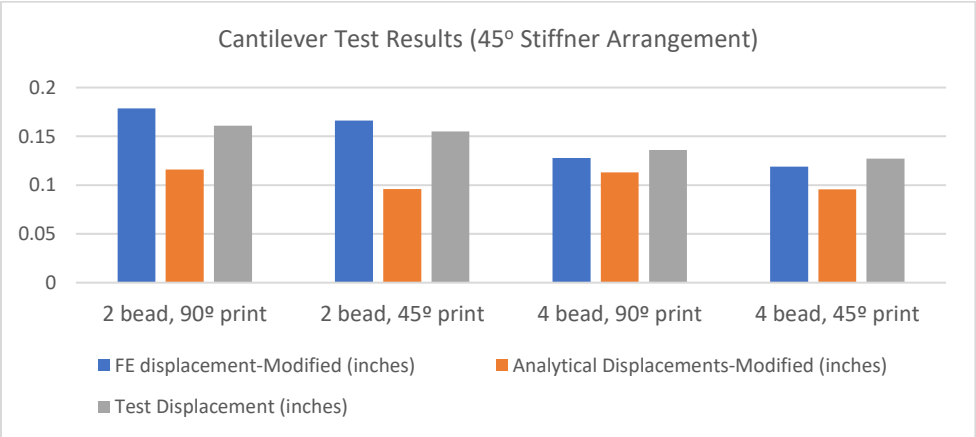

Figure 30-Cantilever test result comparison (45º stiffener arrangement)

Chapter 5 Conclusion and Future Work

The objective of this work was to develop an analytical model which would account for 3D printing orientation of the plates to predict the mechanical behavior of thin wall structure e.g. deflection. The tensile coupon testing methodology was incorporated to study the effect of print orientation on material continuity and stiffness. The previous work [16] does not incorporate the coupon level testing data to validate the effect of 3D print orientation effect on the overall plate structure. In addition, in this work the FE models uses the modulus obtained from the coupon level data to get deflection results. From Table 5, it is seen that the there is large variation between FE results and Analytical results for 90^o configuration of cantilever tests with 0^o stiffener arrangement. For all other configurations, the all three results i.e. FE -Modified, Analytical-Modified and Test results are much closer.

From result section it can be concluded that the 2,4-bead, 90^o orientation, analytical results show some noticeable difference when compared to FE and Test results. Some more in detail work is needed to find out why there is variation for 90^o print orientation. The results are compared with FE and analytical results by using published material properties values [23]. From the discussion in previous section, it can be concluded that the published values show lower displacement as compared to results from coupon level test data. This noticeable reduction in deflection occurs shows how 3D print orientation alters the modulus of a 3D printed structure. This concludes that there is need to develop a methodology which accounts for these affects. This validates that the Analytical model

accounts the effect of 3D-print orientation and can predicts the structural behavior of the plate with some degree of errors.

Next work can be done to calibrate the analytical model so that the data of tensile tests can be compared with the published values. Since there is variation in printing process parameters like layer thickness, printing speed, extruding temperature etc. More tensile coupons can be printed with the same printing parameters as the published values to compare and study the difference between modulus of published values and modulus from the tensile test of coupons. Changes in printing process parameter, geometry of the specimen like width, length, and thickness can change the value of the modulus.

Once the tensile coupons are printed with exact same process parameters as published values, then all the FE models can also be updated with the new modulus. This will be a further addition to get accurate results from the FE models.

The analytical model is derived on the assumption of the beam theory which only considers one dimensional effect, but in actual it is a plate and therefore, model should consider effect of loading in both X and Y directions. Next work can be done to develop the model as per the plate theory assumptions and not using beam theory. Since, the analytical model neglects the twist effect due to unsymmetrical arrangement of the plates (45^o stiffener arrangement), work can be done in developing the formulation which will consider the twisting effect due to asymmetric geometry of the plate. The model does not consider the experimental value of shear modulus (G_{12}) and poisons ratio (ν) for the material for the cases of different print orientations. So, in next work these parameters cane

be determined experimentally so that the analytical model can account for the 100% of the print orientations.

The cantilever test done was not as per the standards. There can be more work done to get accurate results from the tests specially for the cantilever beam test. The cantilever test can be done according to the ASTM D747 standards.

The work can be continued by changing the thickness of the stiffeners and angle of the stiffeners or geometry to study what effect it has on the overall stiffness of the plate and perform more tests with different configurations to compare the results and find exactly which parameter affects the calibration of the analytical model.

Chapter 6 References

[1] S. H. Ahn, M. Montero, D. Odell, S. Roundy and P. K. Wright, "Anisotropic Material Properties of Fused Deposition Modeling ABS," *Rapid Prototyping 8(4)*, pp. 248-257, 2002.

[2] Bellini, Anna and S. Güçeri, "Mechanical Characterization of Parts Fabricated Using Fused Deposition Modeling," *Rapid Prototyping Journal 9.4*, pp. 252-264, 2003.

[3] J. Riddick, A. Hall, H. Mulugeta , R. V. Wahlde, D. Cole and S. Biggs, "Effect of Manufacturing Parameters on Failure in Acrylonitrile-butadiane-styrene Fabricated by Fused Deposition Modeling," in *53rd AIAA/ASME/ASCE/AHS/ASC Structures, Structural Dynamics and Materials Conference*, Honolulu, HI, 2012.

[4] C. Ziemian, M. Sharma and S. Ziemian, "Anisotropic Mechanical Properties of ABS Parts Fabricated by Fused Deposition Modelling," Mechanical Engineering, Murat Gokcek (Ed.),InTech, 2012.

[5] S. M. O. Ziemian and Constance Wilkens Ziemian, "Tensile and Fatigue Behavior of Layered Acrylonitrile Butadiene Styrene," *Rapid Prototyping Journal 21.3*, pp. 270-278, 2015.

[6] J. Lee and A. Huang, "Fatigue Analysis of FDM Materials," *Rapid Prototyping Journal 19.4*, pp. 291-299, 2013.

[7] K. P. Motaparti, "Effect of Build Parameters on Mechanical Properties of Ultem 9085 Parts by Fused Deposition Modeling," Master's Thesis, Missouri University of Science and Technology, 2016.

[8] R. Patel, H. N. Shah and S. V. Kumari, "Experimental Investigation of Fracture of ABS Material by ASTM D-5045 for Different Crack Length & Layer of Orientation Using FDM Process," *International Journal of Mechanical and Industrial Technology,* vol. 3, no. 1, pp. 79-83, 2015.

[9] H. Zhang, "Characterization of Tensile, Creep, and Fatigue Properties of 3D Printed Acrylonitrile Butadiene Styrene," Master's Thesis, Purdue University Indianapolis, 2016.

[10] Sayre III and A. Robert, "Comparative Finite Element Stress Analysis of Isotropic and Fusion Deposited 3D Printed Polymer," Master's Thesis, Rensselaer Polytechnic Institute Hartford, 2014.

[11] El-Gizawy, A. Sherif, C. Shan and B. Graybill, "Process-induced Properties of FDM Products," in *ICMET, International Conference on Mechanical Engineerings and Technology Congress & Exposition*, 2011.

[12] C. Casavola, A. Cazzato, V and C. Pappalettere, "Orthotropic mechanical properties of fused deposition modelling parts described by classical laminate theory," *Materials & Design,* vol. 90, pp. 453-458, 2016.

[13] R. Rane, "Enhancing Tensile Strength of FDM parts using Thermal Annealing and," Master's Thesis, The University of Texas at Arlington, 2018.

[14] I. Gibson, D. Rosen and B. Stucker, Additive Manufacturing Technologies 3D Printing, Rapid Prototyping, and Direct Digital Manufacturing, Springer, 2015.

[15] Sai, Chennakesava and S. Yeole, "Fused Deposition Modelling - Insights".

[16] E. Mares, "PROCESS CALIBRATION FOR ELASTICALLY SCALED 3D PRINTED MODELS USING FUSED DEPOSITION MODELING," Master's Thesis, The University of Texas at Arlington, 2018.

[17] S. Lira, C. Lea and Taylor, "Design Optimization, Fabrication, and Testing of 3D Printed Aircraft Structure Using Fused Deposition Modeling," in *SFF Symposium*, 2018.

[18] C. Ziemian, M. Sharma and S. Ziemian, "Anisotropic mechanical properties of ABS parts fabricated by fused deposition modelling," Mechanical engineering. InTech, 2012.

[19] R. Taylor, E. Mares , R. Rane and M. Love, "Process Calibration for Elastically Scaled 3D Printed Models Using Fused Deposition Modeling," in *2019 AIAA SciTEch Forum,* San Diego, CA, Jan 2019.

[20] H.-J. Chen and S. W. Tsai, "Analysis and Optimum Design of Composite Grid Structures," *Journal of Composite Materials*, vol. 30, 1996.

[21] I. M. Daniel and O. Ishai, Engineering Mechanics of Composite Materials, Oxforf University Press, 2006.

[22] J. Whitney, Structural Analysis of Laminated Anisotropic Plates, Technomic Publishing AG, 1987.

[23] Strarasys, [Online]. Available: http://www.stratasys.com/-/media/files/material-spec-sheets/mss_fdm_absm30_1117a.pdf.